Active Power Filter Control With Vibrating Coordinates Transformation

Sebastian Wodyk and Grzegorz Iwanski, *Senior Member, IEEE*

***Abstract*—This paper presents a control system of an active power filter (APF) based on vibrating reference frame transformation. The proposed vibrating reference frame provides a representation of non-sinusoidal quantities (here the active filter current vector) in the form of sinusoidal signals in a stationary frame, and thanks to that, DC signals are achieved in a *dq* synchronously rotating frame. The article presents theoretical analysis as well as simulation and experimental tests.**

***Index Terms*—Active power filter, vibrating reference frame, power quality.**

Nomenclature

i_F	Active power filter current.
i_{FABC}	Three-phase active power filter current.
$i_{F\alpha\beta}$	Active power filter current $\alpha\beta$ components in a stationary reference frame.
i^*_F, i^{*q}_F	Reference active power filter current and its delay by $\pi/2$ vector.
$i^*_{F\alpha\beta}$, $i^{*q}_{F\alpha\beta}$	Reference active power filter current $\alpha\beta$ components in a stationary reference frame and their delayed by $\pi/2$ components.
$i^*_{F1\alpha\beta}$, $i^*_{F5\alpha\beta}$, $i^*_{F7\alpha\beta}$, $i^*_{F11\alpha\beta}$, $i^*_{F13\alpha\beta}$	Stationary $\alpha\beta$ reference frame components of 1st, 5th, 7th, 11th and 13th reference active power filter current harmonics.
i_{base}	Vibrating reference frame current vector length, rms value of a reference active power filter current scaled by $\sqrt{2}$.
$\lvert i^*_{F1}\rvert$, $\lvert i^*_{F5}\rvert$, $\lvert i^*_{F7}\rvert$, $\lvert i^*_{F11}\rvert$, $\lvert i^*_{F13}\rvert$	Reference active power filter 1st, 5th, 7th, 11th and 13th current harmonics vectors length.
di^*_F, di^{*q}_F	Signal corresponding to the derivative of reference current and its delayed vector
$di^*_{F\alpha\beta}$, $di^{*q}_{F\alpha\beta}$	Signals corresponding to the derivative of reference current $\alpha\beta$ components in a stationary reference frame and their delayed by $\pi/2$ components.
di_{base}	rms value of signal corresponding to the derivative of reference current scaled by $\sqrt{2}$.
i_L	Non–linear load current.
i_{Lh}	Non–linear load harmonic current.
i_{LABC}	Three–phase non–linear load current.
$i_{L\alpha\beta}$	Non–linear load current $\alpha\beta$ components in a stationary reference frame.
$i_{L1\alpha\beta}$, $i_{L5\alpha\beta}$, $i_{L7\alpha\beta}$, $i_{L11\alpha\beta}$, $i_{L13\alpha\beta}$	Stationary $\alpha\beta$ reference frame components of 1st, 5th, 7th, 11th and 13th non–linear load current harmonics.
u_{gABC}	Three-phase grid voltage.
$u_{g\alpha\beta}$	Grid voltage $\alpha\beta$ components in a stationary reference frame.
$\lvert u_g\rvert$	Grid voltage vector length.
ωt	Grid voltage phase angle.
T	Direct transformation matrix from a classic stationary reference frame to a vibrating reference frame.
T_{inv}	Inverse transformation matrix from a vibrating reference frame to a stationary reference frame.
i'_F	Active power filter current in a vibrating reference frame.
$i'_{F\alpha\beta}$	Active power filter current $\alpha'\beta'$ components in a vibrating reference frame.
i'_{Fdq}	Active power filter current *dq* components in a rotating reference frame, obtained from a vibrating reference frame with Park's transformation.
I_{rmsMAX}	Maximal rms value of converter current.
$I_{FhrmsMAX}$	Maximal rms value of active power filter harmonic current.
I_{Fhrms}	rms value of active power filter harmonic current.
I^*_{Fhrms}	rms value of reference active power filter harmonic current.
I_{Lhrms}	rms value of non–linear load harmonic current.
i^*_{Fdq}	*d* component of fundamental active power filter current harmonic in a rotating reference frame oriented along grid voltage vector.

Manuscript received 8 December 2021; revised 26 April 2022; accepted 2 July 2022. Date of publication 11 July 2022; date of current version 24 January 2023. This work was supported by the National Science Centre (Poland) within the Project under Grant 2016/23/B/ST7/03942. Paper no. TPWRD-01816-2021. *(Corresponding author: Sebastian Wodyk.)*

The authors are with the Faculty of Electrical Engineering, Institute of Control and Industrial Electronics, Warsaw University of Technology, 00-662 Warszawa, Poland (e-mail: sebastian.wodyk.dokt@pw.edu.pl; iwanskig@isep.pw.edu.pl).

Color versions of one or more figures in this article are available at https://doi.org/10.1109/TPWRD.2022.3189782.

Digital Object Identifier 10.1109/TPWRD.2022.3189782

$\theta_5, \theta_7, \theta_{11}, \theta_{13}$	Phase shifts of reference active power filter current harmonics.
mode	Signal responsible for switching between a vibrating reference frame and a stationary reference frame.
$I_{\min}$.	Minimal reference active power filter rms current scaled by $\sqrt{2}$ allowing for switch to a vibrating reference frame.
margin	Variable corresponding to the direct transformation denominator.
k_{margin}	Scaling factor for *margin*.
τ_m	Time for which the direct transformation denominator must be greater than *margin*.
u_{DC}	DC–bus voltage.
u^*_{DC}	Reference DC–bus voltage.
i_g	Grid current.
L_L	Inductance of non-linear load filter.
L_F	Inductance of APF filter.
Z_g	Grid impedance.
R_L	Non-linear load DC resistance.
C_{DC}	DC-bus capacitance.
I_{out_dq}	Integrator outputs.
$\mathbf{I}$	Identity matrix.
APF	Active power filter.
BPF	Band-pass filter.
LPF	Low-pass filter.
HPF	High-pass filter.
FFT	Fast Fourier transform.
THD	Total harmonic distortion.

I. Introduction

AMONG many devices connected to the power grid, the non-linear load is especially unfavorable because it strongly affects power quality, due to generation of current harmonics. A significant share in power quality degradation lies with three-phase diode and thyristor rectifiers, which are widely used in industry due to low cost and high reliability. Moreover, some share of the harmonics proliferation belongs to residential areas [1]. In order to reduce their impact on the power system, many methods have been proposed, which in general can be divided into passive and active.

Active methods, based on power electronic converters, have many advantages over passive methods, e.g., smaller weight and volume, wider application flexibility, reduced resonance issues, better filtering performance [2], [3]. In the case of compensation harmonics in a three-phase system, active filtering may be performed with a three-phase voltage source converter connected to the grid near the source of harmonics. Such a configuration is known as a shunt active power filter (APF) and is presented in Fig. 1. Proper operation of APF requires high accuracy, which depends on current reference determination, and on the other hand, on the accuracy of the inner current control loop.

Current harmonics may be extracted from instantaneous power components *pq* [4], using high-pass filtering. A similar approach is high-pass filtering of synchronous reference frame

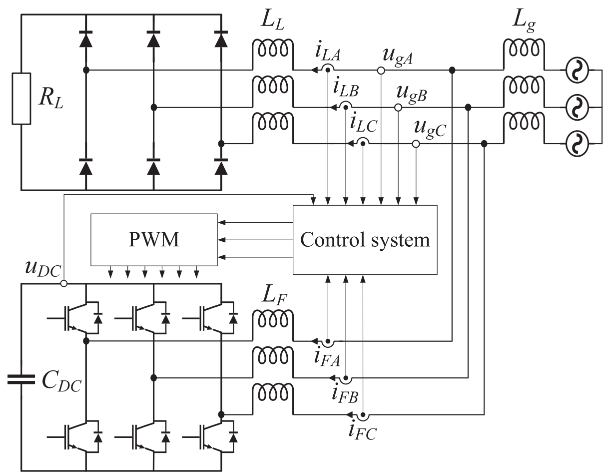

Fig. 1. Scheme of a shunt APF operating with a six-pulse diode rectifier.

dq currents [5]–[7], where the grid voltage phase angle is used for transformation. For both *pq* power based and *dq* current based harmonics detection, reference signals consist mainly of harmonics the frequencies of which are 6*n* times fundamental frequency, where *n* is a positive integer, and some DC part responsible for maintaining voltage in the converter DC–bus. Another approach is stationary frame current harmonics detection [8]; then the reference current contains harmonics of frequency $6n\pm1$, and some part of fundamental harmonic. This solution is useful especially in single phase systems, however with consideration of different frequencies [9].

Current harmonics detection, independently of the chosen method, is a challenging issue in digital control systems, due to delays caused by signal processing [5], [10], [11]. Therefore, switching frequency (as well as sampling frequency), should be as high as possible in order to reduce the impact of these delays on filter performance.

As the reference signals are not DC or sinusoidal, it is not trivial to achieve accurate tracking. One of the methods is utilization of classic proportional-integral (PI) controllers [4], [11], [12], though it is known that they cannot achieve zero steady state error for non-DC reference. Another approach is to use hysteresis controllers [13]–[15], which introduces some drawbacks like variable switching frequency.

Constant switching frequency may be obtained using a variable hysteresis band, which was proposed for a predictive control system [16], but such systems require precise knowledge on converter parameters and are computationally expensive. PI controllers may be applied also in a multiple reference frame, which rotates synchronously with each harmonic. The authors of [17] applied such a system in a series APF. In case of shunt filters, similar systems were used for reference generation [18]–[20], but not in an inner current control loop. Although a solution like that provides zero steady state error for selected harmonics, it implies controllers limitation problems, because realization of anti- windup in a structure of several parallel-connected terms is not trivial.

Another solution for selected harmonics control are oscillatory terms in controllers [6]–[8], [20], which may be applied both in a stationary frame and in a synchronously rotating frame. Then, output of each oscillatory term should be sinusoidal, which induces further issues associated with controllers limitation. Moreover, tuning of control systems containing parallel-connected resonant terms cannot be done in a simple way, and requires often heuristic methods like particle swarm optimization [21].

Recently a new stationary frame transformation, called vibrating coordinates transformation, has been proposed [22]. It allows to represent a distorted vector (containing harmonics and negative sequence component) in the form of a new vector which creates a circular hodograph. Then the control system can be built basing on PI controllers, because vector components representation in a synchronous frame are the DC signals, as presented in the cited reference. APF reference current is clearly an example of a distorted vector.

This paper presents a novel approach to shunt APF control, which applies vibrating coordinates transformation. The main assumption of a control system is utilization of PI controllers, in such a way that the proportional term is applied in the stationary reference frame and the integral term is applied in the synchronous reference frame. Another contribution is the current limitation method, which is consequently omitted by authors. The paper presents theoretical analysis as well as simulation and experimental studies.

II. Theoretical Analysis

A. Direct and Inverse Transformation

According to [22], APF current i_F can be represented in vibrating coordinates using the following transformation matrix:

$$T = \frac{i_{base}}{|u_g|\left(i^*_{F\alpha} i^{*q}_{F\beta} - i^{*q}_{F\alpha} i^*_{F\beta}\right)} \times \begin{bmatrix} u_{g\alpha} i^{*q}_{F\beta} - u_{g\beta} i^*_{F\beta} & -u_{g\alpha} i^{*q}_{F\alpha} + u_{g\beta} i^*_{F\alpha} \\ u_{g\alpha} i^*_{F\beta} + u_{g\beta} i^{*q}_{F\beta} & -u_{g\alpha} i^*_{F\alpha} - u_{g\beta} i^{*q}_{F\alpha} \end{bmatrix} \quad (1)$$

where: u_g – grid voltage, i^*_F – reference APF current, i^{*q}_F – reference APF current delayed by $\pi/2$, i_{base} – rms value of i^*_F scaled by $\sqrt{2}$ (base vector length in a vibrating reference frame).

In order to achieve appropriate control signals, which for grid connected converters represent voltage drop across inductor reactance, an inverse transformation matrix is used:

$$T_{inv} = \frac{1}{|u_g|\, di_{base}} \times \begin{bmatrix} u_{g\alpha} di^{*q}_{F\alpha} - u_{g\beta} di^*_{F\alpha} & u_{g\alpha} di^*_{F\alpha} + u_{g\beta} di^{*q}_{F\alpha} \\ u_{g\alpha} di^{*q}_{F\beta} - u_{g\beta} di^*_{F\beta} & u_{g\alpha} di^*_{F\beta} + u_{g\beta} i^{*q}_{F\beta} \end{bmatrix} \quad (2)$$

where di^*_F, di^{*q}_F – signal corresponding to derivative of reference current and its delayed vector, di_{base} – rms value of di^*_F, scaled by $\sqrt{2}$.

In order to provide correct delays between i^*_F and i^{*q}_F, as well as to determine di^*_F and di^{*q}_F, decomposition of the reference filter current, taking into account the order of harmonic which should be filtered is necessary. Considering compensation of 5th, 7th, 11th and 13th harmonic, signals can be reconfigured as:

$$i^*_{F\alpha} = i^*_{F1\alpha} + i^*_{F5\alpha} + i^*_{F7\alpha} + i^*_{F11\alpha} + i^*_{F13\alpha} \quad (3a)$$

$$i^*_{F\beta} = i^*_{F1\beta} + i^*_{F5\beta} + i^*_{F7\beta} + i^*_{F11\beta} + i^*_{F13\beta} \quad (3b)$$

$$i^{*q}_{F\alpha} = i^*_{F1\beta} - i^*_{F5\beta} - i^*_{F7\beta} + i^*_{F11\beta} + i^*_{F13\beta} \quad (4a)$$

$$i^{*q}_{F\beta} = -i^*_{F1\alpha} + i^*_{F5\alpha} + i^*_{F7\alpha} - i^*_{F11\alpha} - i^*_{F13\alpha} \quad (4b)$$

$$di^*_{F\alpha} = -i^*_{F1\beta} + 5i^*_{F5\beta} - 7i^*_{F7\beta} + 11i^*_{F11\beta} - 13i^*_{F13\beta} \quad (5a)$$

$$di^*_{F\beta} = i^*_{F1\alpha} - 5i^*_{F5\alpha} + 7i^*_{F7\alpha} - 11i^*_{F11\alpha} + 13i^*_{F13\alpha} \quad (5b)$$

$$di^{*q}_{F\alpha} = i^*_{F1\alpha} + 5i^*_{F5\alpha} - 7i^*_{F7\alpha} - 11i^*_{F11\alpha} + 13i^*_{F13\alpha} \quad (6a)$$

$$di^{*q}_{F\beta} = i^*_{F1\beta} + 5i^*_{F5\beta} - 7i^*_{F7\beta} - 11i^*_{F11\beta} + 13i^*_{F13\beta} \quad (6b)$$

Description of $\alpha\beta$ current and its derivatives, forming the basis of the calculation, is presented in the Appendix.

Determination of the reference current harmonics may be done by filtration of load current i_L, as shown in Fig. 2. The presented filtration structure ensures low coupling between respective harmonic, which allows to achieve high attenuation of unwanted frequencies, maintaining satisfactory dynamics. Fig. 3. presents the Bode plot of the proposed current harmonics detection structure, for parameters presented in Table I. Magnitude gain for each path is 0 dB for its frequency, and the phase shift is zero.

Fundamental harmonic of the reference APF current is the result of DC–bus voltage regulation, like in classical voltage

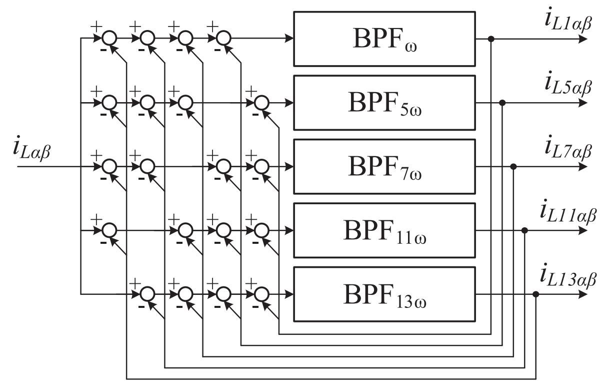

Fig. 2. Load current filtration and harmonics decomposition.

TABLE I
Parameters of Filters Used for Current Decomposition

Symbol	Transfer function
BPF_{ω}	$G(s) = \frac{s100\pi}{s^2 + s100\pi + (100\pi)^2}$
$BPF_{5\omega}$	$G(s) = \frac{s100\pi}{s^2 + s100\pi + (500\pi)^2}$
$BPF_{7\omega}$	$G(s) = \frac{s100\pi}{s^2 + s100\pi + (700\pi)^2}$
$BPF_{11\omega}$	$G(s) = \frac{s100\pi}{s^2 + s100\pi + (1100\pi)^2}$
$BPF_{13\omega}$	$G(s) = \frac{s100\pi}{s^2 + s100\pi + (1300\pi)^2}$

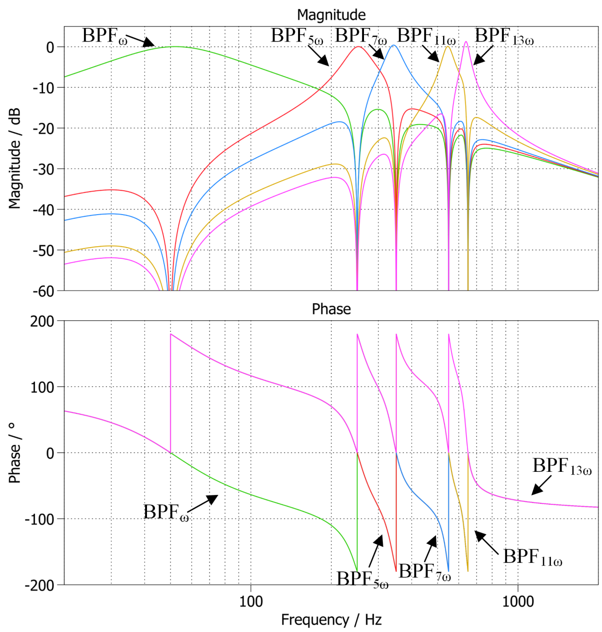

Fig. 3. Bode plot of the filtration structure.

oriented control systems. When all components of a reference current are determined, i_{base} and di_{base} can be calculated in the following manner:

$$i_{base} = \sqrt{|i^*_{F1}|^2 + |i^*_{F5}|^2 + |i^*_{F7}|^2 + |i^*_{F11}|^2 + |i^*_{F13}|^2} \quad (7)$$

$$di_{base} = \sqrt{|i^*_{F1}|^2 + 25|i^*_{F5}|^2 + 49|i^*_{F7}|^2 + 121|i^*_{F11}|^2 + 169|i^*_{F13}|^2} \quad (8)$$

Such an assignment of i_{base} causes that current vector length in a vibrating reference frame will be proportional to $\sqrt{2}I_{FRMS}$. It should be noted that any vector in a stationary $\alpha\beta$ frame, if it contains no harmonics and negative sequence, meets this assumption. As the content of the respective harmonic in the control signal is higher by its order, because it is proportional to the voltage drop through an APF inductor, di_{base} is selected in a similar manner, taking into account the number of each harmonic. Then the APF current in a vibrating reference frame i'_F is expressed as:

$$\begin{bmatrix} i'_{F\alpha} \\ i'_{F\beta} \end{bmatrix} = T \begin{bmatrix} i_{F\alpha} \\ i_{F\beta} \end{bmatrix} = \begin{bmatrix} i_{base}\cos(\omega t) \\ i_{base}\sin(\omega t) \end{bmatrix} \quad (9)$$

where ωt stands for the grid voltage phase angle. Further transformation to the rotating reference frame gives the following result:

$$\begin{bmatrix} i'_{Fd} \\ i'_{Fq} \end{bmatrix} = \begin{bmatrix} \cos(\omega t) & \sin(\omega t) \\ -\sin(\omega t) & \cos(\omega t) \end{bmatrix} \begin{bmatrix} i_{base}\cos(\omega t) \\ i_{base}\sin(\omega t) \end{bmatrix} = \begin{bmatrix} i_{base} \\ 0 \end{bmatrix} \quad (10)$$

Basing on (10) the reference current in the *dq* frame is equal to i_{base} in the *d* axis and to 0 in the *q* axis.

B. Current Limitation

The important feature of APF is maximal apparent power, which strictly depends on the converter rms current. Since current is the result of the control system operation, its rms value limitation needs to be taken into consideration. It should be noted that this issue is consistently omitted by the authors. In general, calculation of the rms value of a signal requires integration. However, in case of the proposed system the instantaneous value of each harmonic is known, thus the rms value of the reference current can be simply assigned with (7). On the one hand, current limitation is applied in the DC-bus voltage controller, for fundamental harmonic, and on the other hand, compensating current also needs to be limited. It has been assumed that the fundamental harmonic current i_{F1} should have the highest priority, because it is responsible for maintaining the voltage in the DC–bus. Further, the maximal rms value of the harmonic current I_{Fhrms} can be expressed as:

$$I_{FhrmsMAX} = \sqrt{I^2_{rmsMAX} - \frac{|i^*_{F1}|^2}{2}} \quad (11)$$

where I_{rmsMAX} is the maximal converter current rms value.

When the reference harmonic current tends to exceed this value, each harmonic should be recalculated using the scaling factor that ensures the overall current is kept within the limit. The scaling factor is I_{Fhrms} to the actual reference harmonic current ratio. The proposed current limitation structure is presented in Fig. 5. In order to simplify calculation, rms values scaled by $\sqrt{2}$ of all signals are used, which gives the same results. The scaling factor is limited from zero to one. If harmonic current is below the limitation, the scaling factor is equal to one, otherwise it decreases.

The results of the proposed current limitation method are presented in Figs. 5 and 6. Two situations were taken into account, the first one, when the load harmonic current rms value causes reaching the limit, and the second one, when fundamental harmonic current reaches the limit. As it can be observed, fundamental harmonic has the highest priority, as $i^*{}_{F1d}$ rises, the rms value of harmonic current decreases in order to match the limit.

C. Transformation Constraints

Seeing that calculation of coefficients for both direct and inverse transformation requires division by varying terms, related to the reference current, some constraints need to be imposed in order to avoid division by zero, and in consequence, instability of the system. For this purpose, switching between two modes, from which the first is classical *dq* control, and the second one is the use of the vibrating reference frame transformation. Mode selection depends on the instantaneous value of the term $i^*_{F\alpha} i^{*q}_{F\beta} - i^{*q}_{F\alpha} i^*_{F\beta}$, as well as the rms value of the reference current, expressed as i_{base}. In general it can be described as (12) shown at the bottom of the next page, which consists of DC component and oscillating parts. It crosses zero when the reference current is equal to zero, or when the oscillating part

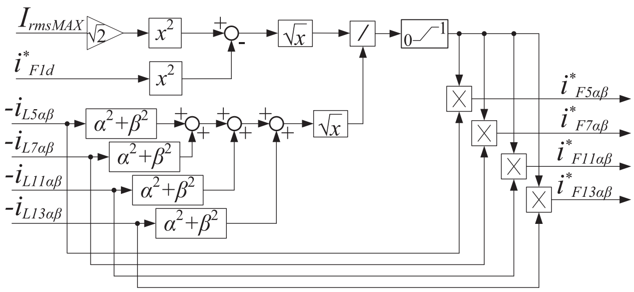

Fig. 4. Scheme of the current limitation structure.

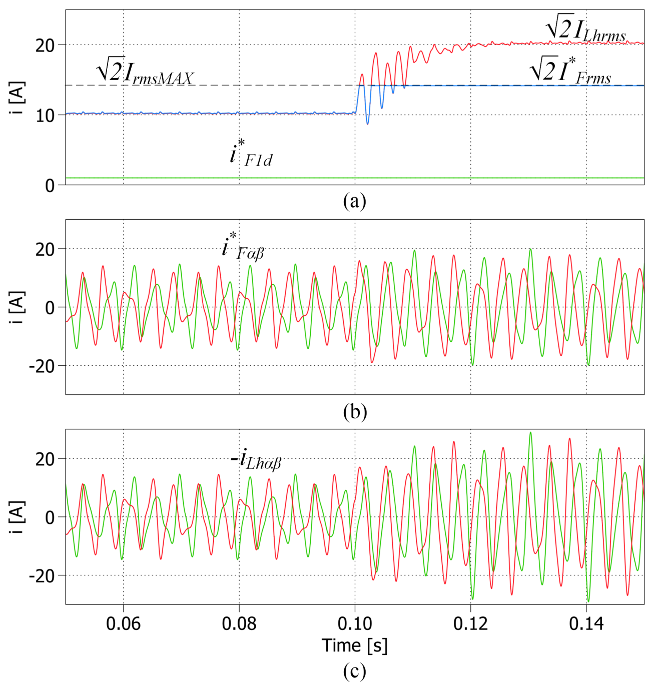

Fig. 5. Current limitation in case of load harmonic current change and constant fundamental harmonic current, (a) I_{rmsMAX} – maximal rms value of APF current, I_{Lhrms} – rms value of load harmonic current, I^*_{Frms} – rms value of reference APF current, i^*_{F1d} – reference fundamental harmonic of APF current in a classical rotating reference frame, (b) $i^*_{F\alpha\beta}$ - overall reference APF current in a stationary $\alpha\beta$ reference frame, (c) $i_{L\alpha\beta}$ - non-linear load harmonic current in a stationary $\alpha\beta$ reference frame.

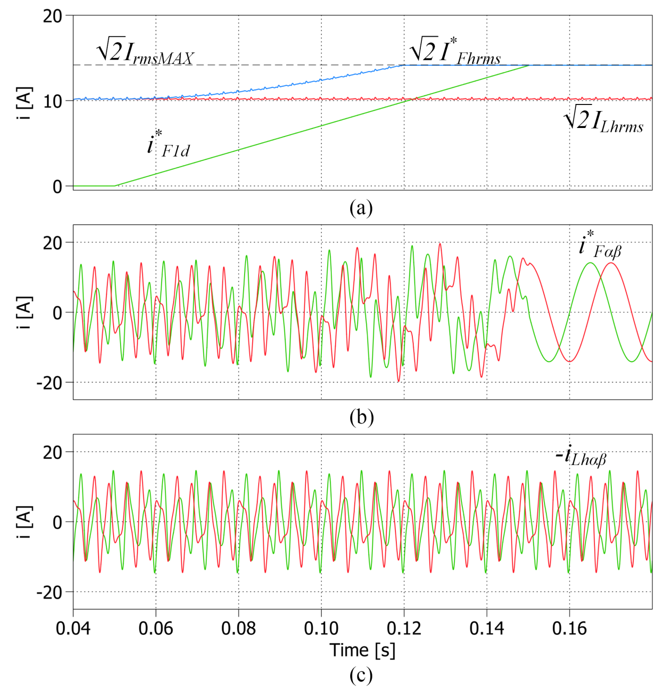

Fig. 6. Current limitation in case of constant load harmonic current and linear change of fundamental harmonic current, (a) I_{rmsMAX} – maximal rms value of APF current, I_{Lhrms} – rms value of load harmonic current, I^*_{Frms} – rms value of reference APF current, i^*_{F1d} – reference fundamental harmonic of APF current in a classical rotating reference frame, (b) $i^*_{F\alpha\beta}$ - overall reference APF current in a stationary $\alpha\beta$ reference frame, (c) $i_{L\alpha\beta}$ - non-linear load harmonic current in a stationary $\alpha\beta$ reference frame.

magnitude is greater than the DC part, which may occur in transient states, when reference current is changing.

The proposed solution to this problem is the mode selection scheme, dependent on the reference current, which is presented in Fig. 7. Mode switching from the vibrating reference frame ($mode = 1$) to classical dq ($mode = 0$) occurs when one of the two conditions is not met. First, when i_{base} is lower than $I_{\min}$. Second, when the instantaneous value of $|i^*_{F\alpha}i^{*q}_{F\beta} - i^{*q}_{F\alpha}i^*_{F\beta}|$ is too low. It is checked by comparison of this term with *margin*, that is its average value scaled by factor k_{margin}, which is equal to 0.01 in this case. If i_{base} is greater than $I_{\min}$ and $|i^*_{F\alpha}i^{*q}_{F\beta} - i^{*q}_{F\alpha}i^*_{F\beta}|$ is above the *margin* longer than the assumed time τ_m, the system returns to operation in the vibrating reference frame ($mode = 1$). It has been assumed that τ_m is equal to 10 ms. The values of $I_{\min}$, k_{margin} and τ_m were established by trial and error. An example of mode selection operation is presented in Fig. 8.

D. Control System With DC-Bus Voltage Regulation

The proposed control system of APF is presented in Fig. 9. The measured DC–bus voltage passes through low-pass filtration in order to reduce the influence of harmonics to regulation performance. The cut-off frequency is 150 Hz. The output of the DC–bus voltage controller is the reference d component of the fundamental current harmonic, limited to $\sqrt{2}I_{rmsMAX}$, which is transformed to the $\alpha\beta$ frame using the grid voltage angle. Band–pass filtration of the grid voltage reduces the impact of voltage harmonics on angle calculation. Harmonics of the APF reference current are found using load current decomposition (Fig. 2).

$$\begin{aligned} i^*_{F\alpha}i^{*q}_{F\beta} - i^{*q}_{F\alpha}\, i^*_{F\beta} = &-|i^*_{F1}|^2 + |i^*_{F5}|^2 + |i^*_{F7}|^2 - |i^*_{F11}|^2 - |i^*_{F13}|^2 + 2\,|i^*_{F5}|\,|i^*_{F7}|\cos(12\omega t - \theta_5 - \theta_7) \\ &- 2\,|i^*_{F1}|\,|i^*_{F11}|\cos(12\omega t - \theta_{11}) - 2\,|i^*_{F1}|\,|i^*_{F13}|\cos(12\omega t - \theta_{13}) - 2\,|i^*_{F11}|\,|i^*_{F13}|\cos(24\omega t - \theta_{11} - \theta_{13}) \end{aligned} \quad (12)$$

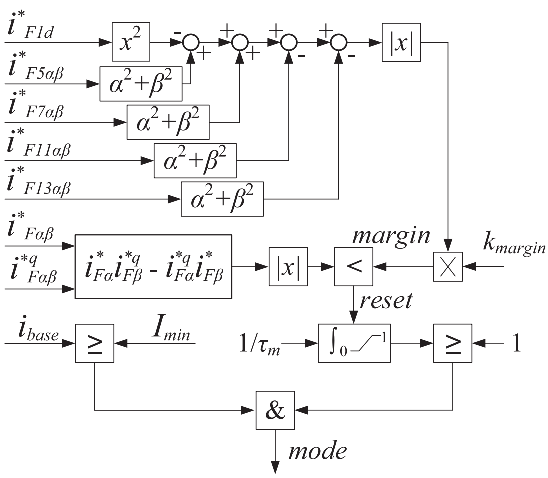

Fig. 7. Scheme of the mode selection structure.

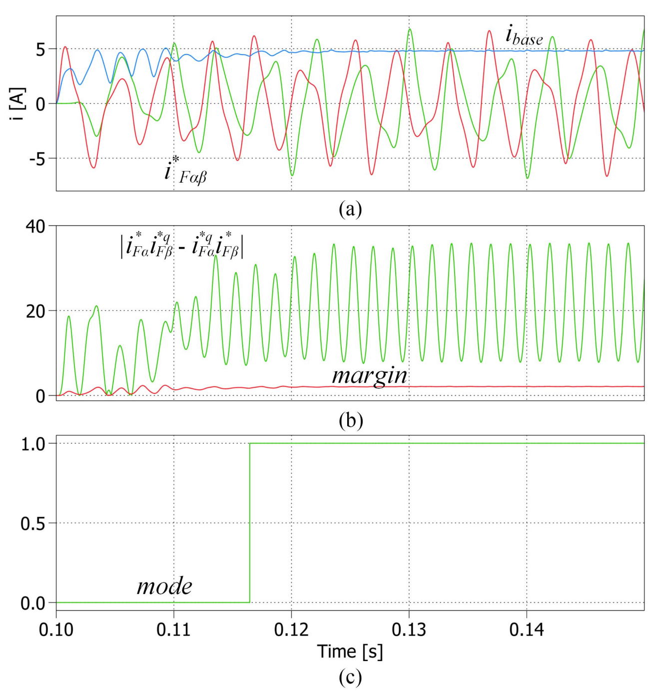

Fig. 8. Mode selection during reference current transient state, (a) i_{base} - vibrating reference frame current vector length, $i^*_{F\alpha\beta}$ - reference active power filter current $\alpha\beta$ components in a stationary reference frame, (b) oscillatory term of the transformation denominator and *margin* related to its constant term, (c) mode switching.

Further total reference current goes through the limitation block (Fig. 4). Limited current is used to calculate transformations coefficients and reference current. Current is regulated both in stationary and synchronous reference frames, such that in the stationary frame a proportional term is used, and in a synchronous frame an integral term is used. Thanks to that, the system is less sensitive to possible inaccuracies that may affect the vibrating reference frame transformation. It should be noted that in ideal conditions, the described current controller is equivalent to the classical PI controller applied in the *dq* frame. If *mode* $= 1$, the vibrating reference frame transformation is used, otherwise classical *dq* control is applied, which is described in

TABLE II
PARAMETERS OF A LABORATORY RIG

Symbol	Quantity	Value
U_{gn}	Nominal grid voltage (L-L rms)	230 V
$I_{FrmsMAX}$	Maximal APF rms current	10 A
L_F	APF chokes inductance	1.7 mH
R_{LF}	APF chokes resistance	40 mΩ
C_{DC}	APF DC-bus capacitance	0.5 mF
U_{DC}	Reference APF DC-bus voltage	410 V
L_L	Load chokes inductance	3 mH
R_L	Load chokes resistance	40 mΩ
S_L	Rated load power	4.3 kVA
f_s	Switching frequency	10 kHz
L_g	Grid inductance	40 µH
R_g	Grid resistance	1 mΩ
L_T	Transformer leakage inductance	1 mH
R_T	Transformer winding resistance	400 mΩ

Section II–C. Finally, the control signal is a sum of controllers output signals and grid voltage feedforward.

III. Simulation and Experimental Results

Simulation and experimental tests were carried out with the use of a laboratory rig configured according to the scheme presented in Fig. 1. Simulated grid voltage contains 3 V of 5th harmonic and 3 V of 7th harmonic, which results in 2.5% voltage total harmonic distortion (THD). For the sake of a non-linear load, a three-phase diode rectifier with an inductive input filter was used, but the proposed control system is feasible for any type of non-linear three-wire load, e.g., frequency converters of AC drives or large AC motors soft–starters, because they are a source of harmonics of frequency $6n\pm1$. It should be noted that filtration of harmonics that are introduced by switched-mode power supplies, e.g., in computer centers, demands a different approach due to a significant share of zero sequence harmonics and single-phase character of a load. APF was realized with a three-phase two-level voltage source converter, built with IGBT transistors. In the experiment, the control system was implemented in a TMS320F28335 microcontroller. The parameters of the examined circuit are presented in Table II.

The results of the simulation are presented in Figs. 10 and 11. The operation of APF may be divided into three stages, as can be seen in Fig. 10. They are: 1) turning on of the converter and DC-bus voltage creation (20 ms), 2) switch on of the harmonic filtration (100 ms) 3) change of load (150 ms). Filtering of current harmonics is enabled when reference voltage in the DC-bus is provided. The simulated load equals 3.3 kVA initially, and 6.3 kVA after step change. As can be noticed, the control system operates omitting the vibrating reference frame (*mode* $= 0$) for some time after the start of the filtering, which is caused by the issues described in Section II–C. Further, when *mode* $= 1$, the vibrating reference frame is applied, and converter current in a new $d'q'$ takes the form of DC signals. The control system reacts quickly to the load change, in time about half of a fundamental harmonic period, which is considered a satisfactory result. Current filtration performance is presented in Fig. 11, APF produces desirable harmonics. As can be noticed,

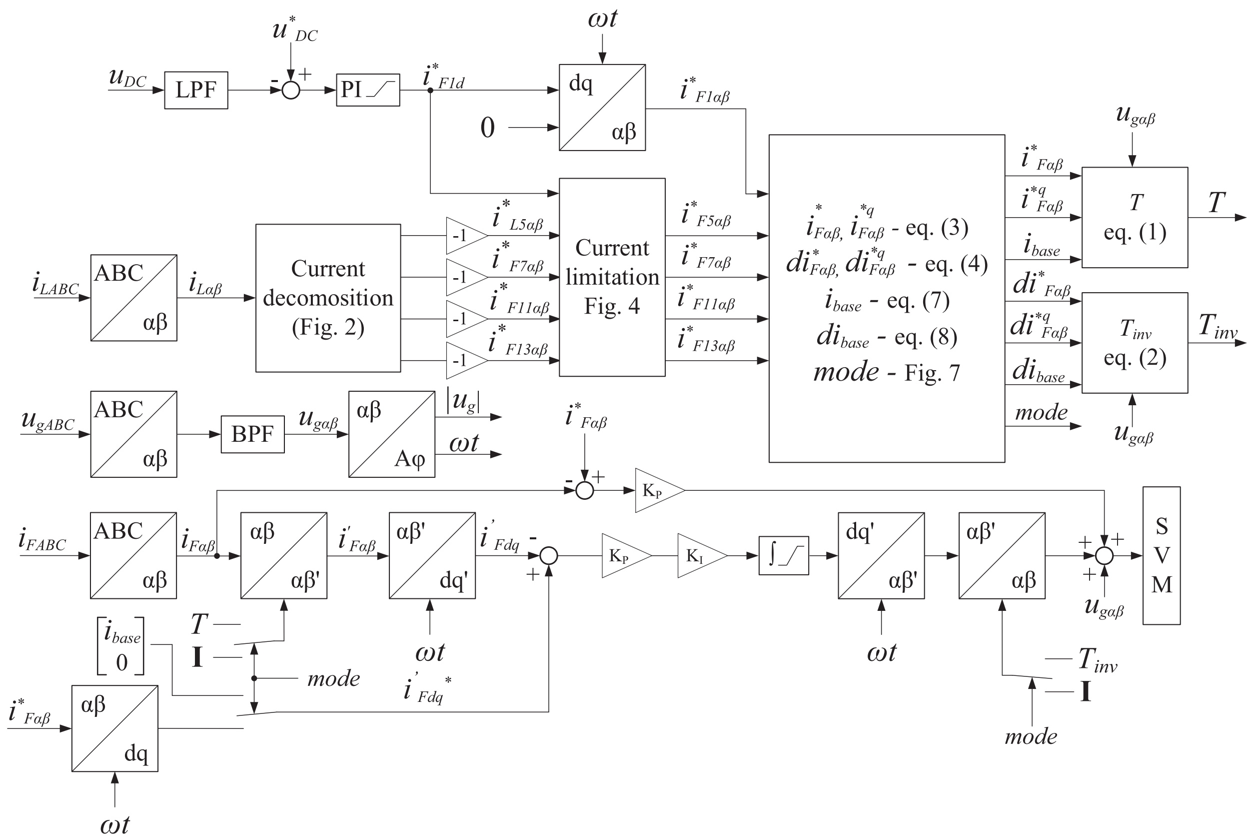

Fig. 9. Scheme of the proposed control system.

turn on of the vibrating reference frame transformation visibly corrects the grid current i_g shape.

Fig. 12 presents comparison of different APF control methods utilizing PI controllers. One of them is control of each harmonic in a synchronous frame rotating with its pulsation (multiple reference frame) [17]. The second one is control in a classical *dq* reference frame, with high–pass filters (HPF) used to determine load harmonic current [10], [11]. Both methods were simulated with the same load and supply parameters as the vibrating reference frame control. As can be seen, the vibrating reference frame features the best dynamic response and the lowest overshoot (in terms of filtered grid current), among the others. This is due to the lack of dynamic terms in the control loop which are needed in multiple reference frame. Decomposition of the measured APF current was done with the filtration structure presented in Fig. 3. On the other hand, the greatest overshoot occurs in classical *dq* control, which is caused by harmonic current detection with second order high–pass filters with 50 Hz cut-off frequency. It should be noted that dynamic performance of such a system may be improved by the use of the higher cut-off frequency, but the cost is the accuracy of the harmonic extraction, especially 5th and 7th.

The steady-state performance of the simulated methods is compared in Table III. The presented current THD contains swathing ripples. The vibrating reference frame reveals slightly better performance than the multiple reference frame, although both methods can theoretically achieve zero steady-state error. However, in the case of the multiple reference frame, band-pass filtration is applied in measurement of load current, as well as filter current, making the system more sensitive to mutual influence of the current harmonics. Multiple reference frame approach demands two control paths for each harmonic, which might lead to issues with multiple controllers tuning as well as with limitation of multiple integrators, whereas in a vibrating reference frame there are only two integration terms. The highest current THD was achieved for a classical *dq* system, which is caused mainly by utilizing PI controllers for tracking strongly oscillating reference, and by attenuation intruded by

TABLE III
THD OF THE SIMULATED CURRENT FOR DIFFERENT APF CONTROL METHODS

Current	Description	THD$_i$
i_{LA}		22.4 %
i_{LB}	Load current	22.4 %
i_{LC}		22.4 %
i_{g1A}		4.9 %
i_{g1B}	Vibrating reference frame	4.9 %
i_{g1C}	control	4.9 %
i_{g2A}		5 %
i_{g2B}	Multiple reference frame	5 %
i_{g2C}	control	5 %
i_{g3A}		5.3 %
i_{g3B}	Classical *dq* control with HPF	5.3 %
i_{g3C}	in a load current measurement	5.3 %

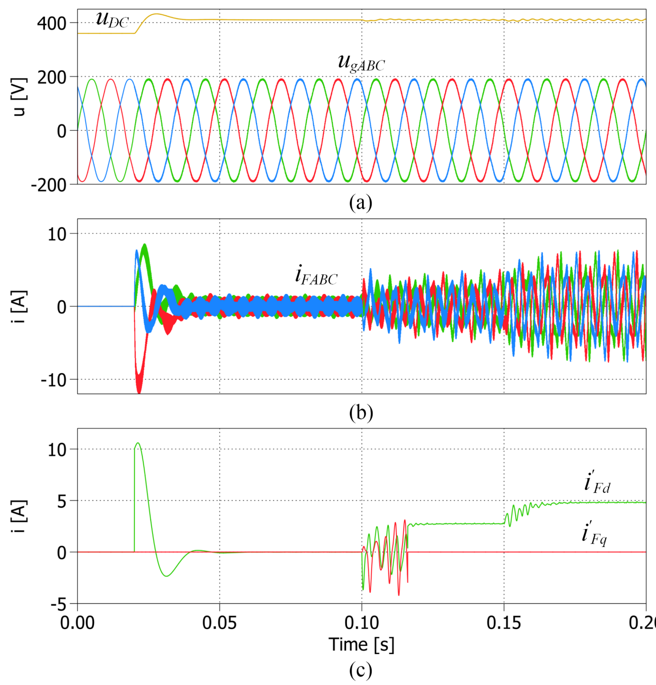

Fig. 10. Simulation results presenting performance of APF, (a) u_{DC} – DC-bus voltage, u_{gABC} – three-phase line–to-neutral grid voltage, (b) i_{FABC} – three-phase APF current, (c) i'_{Fdq} – APF current in the new $d'q'$ frame.

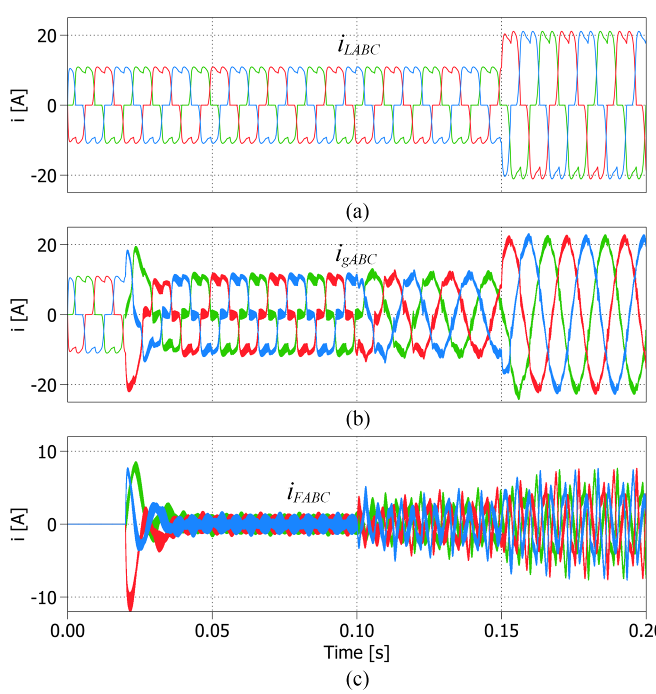

Fig. 11. Simulation results presenting currents in the analyzed circuit, (a) i_{LABC} – three-phase non-linear load current, (b) i_{gABC} – three-phase grid current, (c) i_{FABC} – three-phase APF current.

high-pass filtration to a lesser degree. This method introduces some drawbacks like non-intuitive limitation of the reference APF current, which demands calculation of non-sinusoidal signals rms values, or share of measuring noise in the reference current. Such issues do not concern the vibrating reference frame control and multiple reference frame control, due to access

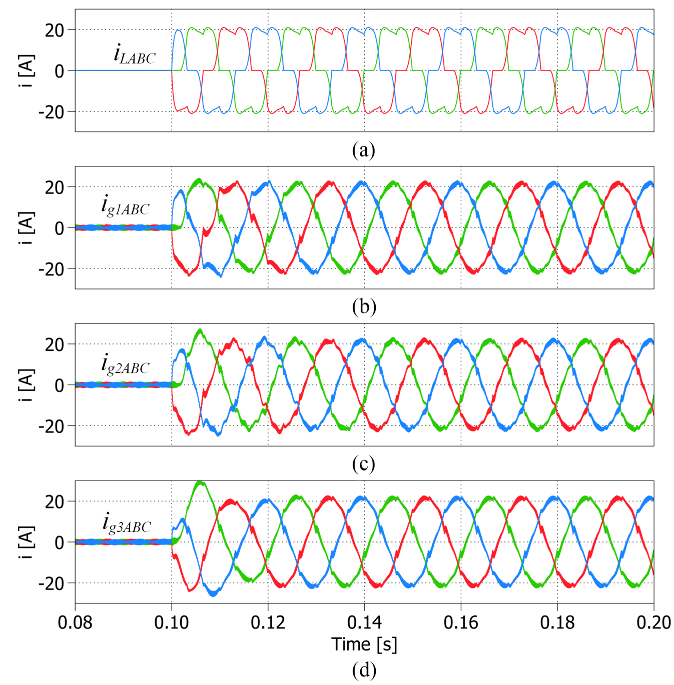

Fig. 12. Simulation results presenting comparison of different APF control methods, (a) i_{LABC} – three-phase non-linear load current, (b) i_{g1ABC}– three-phase grid current for vibrating reference frame control, (c) i_{g2ABC}– three-phase grid current for multiple reference frame control, (d) i_{g3ABC}– three-phase grid current for classical dq control.

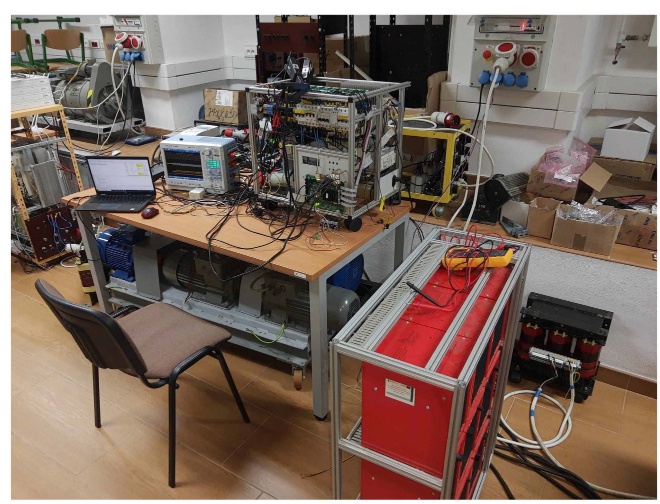

Fig. 13. Laboratory setup used in the experiment.

TABLE IV
THD OF THE MEASURED CURRENT

Current	Description	THD$_i$
i_{LA}	Load current	23.8 %
i_{LB}		23.8 %
i_{LC}		23.9 %
i_{g1A}	Grid current with only P controller	9.3 %
i_{g1B}		10.2 %
i_{g1C}		9.9 %
i_{g2A}	Grid current with full PI controller	5.7 %
i_{g2B}		5.7 %
i_{g2C}		5.2 %

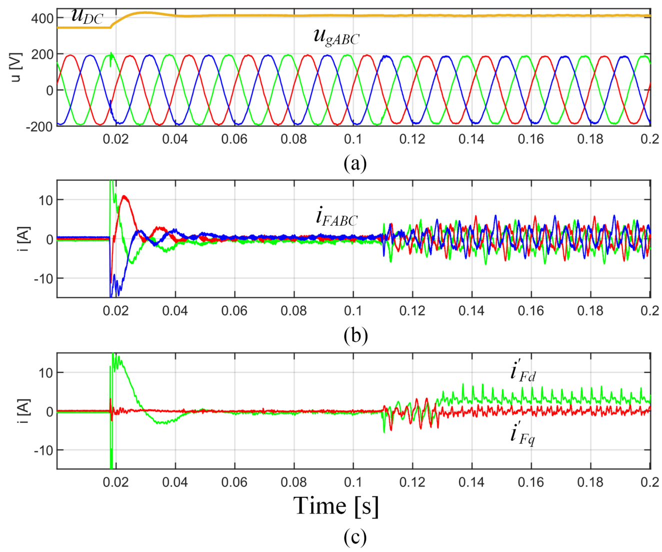

Fig. 14. Experimental results presenting performance of APF, (a) u_{DC} – DC-bus voltage, u_{gABC} – three-phase line–to–neutral grid voltage, (b) i_{FABC} – three-phase APF current, (c) i'_{Fdq} – APF current in the new $d'q'$ frame.

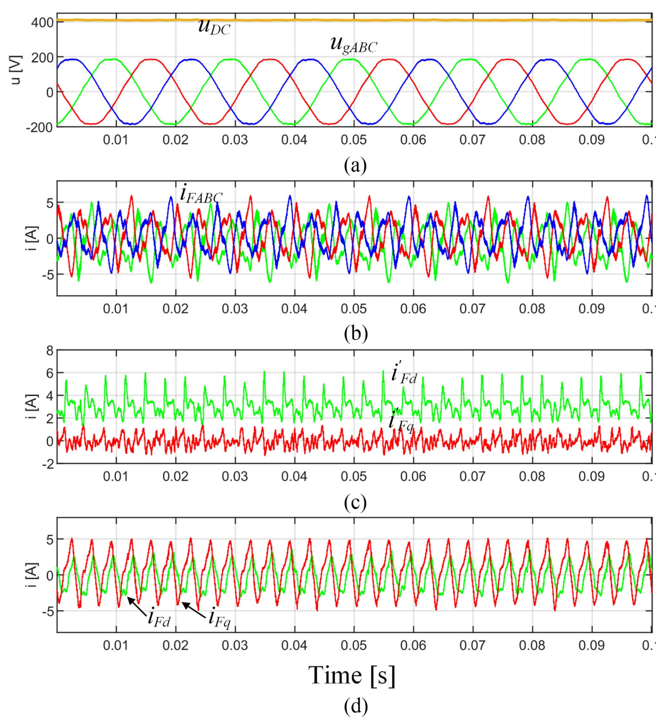

Fig. 15. Experimental results presenting steady-state operation of APF, (a) u_{DC} – DC-bus voltage, u_{gABC} – three-phase line–to–neutral grid voltage, (b) i_{FABC} – three-phase APF current, (c) i'_{Fdq} – APF current in the new $d'q'$ frame, (d) i_{Fdq} – APF current in a classical dq frame.

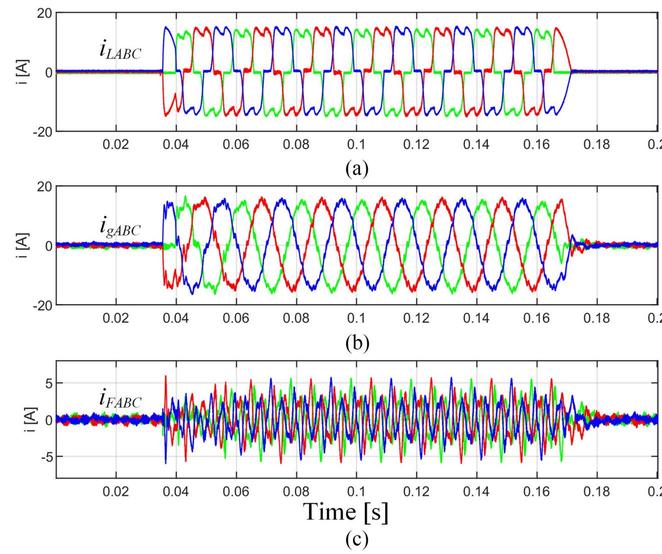

Fig. 16. Experimental results presenting currents in the analyzed circuit, (a) i_{LABC} – three-phase non-linear load current, (b) i_{gABC} – three-phase grid current, (c) i_{FABC} – three-phase APF current.

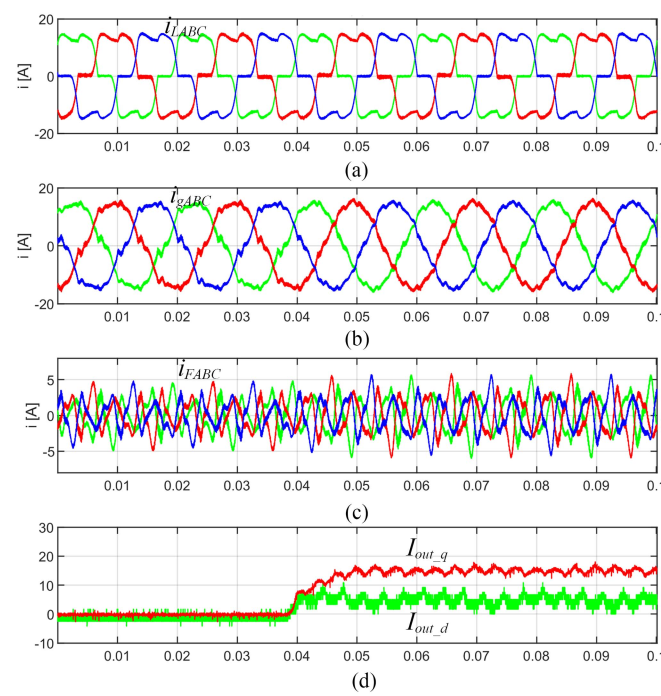

Fig. 17. Experimental results presenting impact of the integration in a new $d'q'$ frame, (a) i_{LABC} – three-phase non-linear load current, (b) i_{gABC} – three-phase grid current, (c) i_{FABC} – three-phase APF current, (d) I_{out-dq} – integrator outputs.

to the each harmonic separately, which allows also selective filtration.

The experiment was carried out in conditions close to simulation; the difference is load power which equals 4.3 kVA, with no step changes, which is caused by limitations of the experimental setup. The laboratory rig was connected to the grid via an 8 kVA 400/230 transformer, which resulted in a much higher grid impedance, approximately equal to transformer impedance (see Table II), and as a consequence, smaller current ripple in the experiment. Results were recorded with a DL850E Scopecorder in the form of data files, oscillograms were prepared using MATLAB for adding appropriate scales. Three-phase load and filter current measurement for the registration purpose was realized with an A622 probe with 100-kHz bandwidth, whereas grid current was achieved as their sum. Synchronous reference current components are visualized from the control unit using

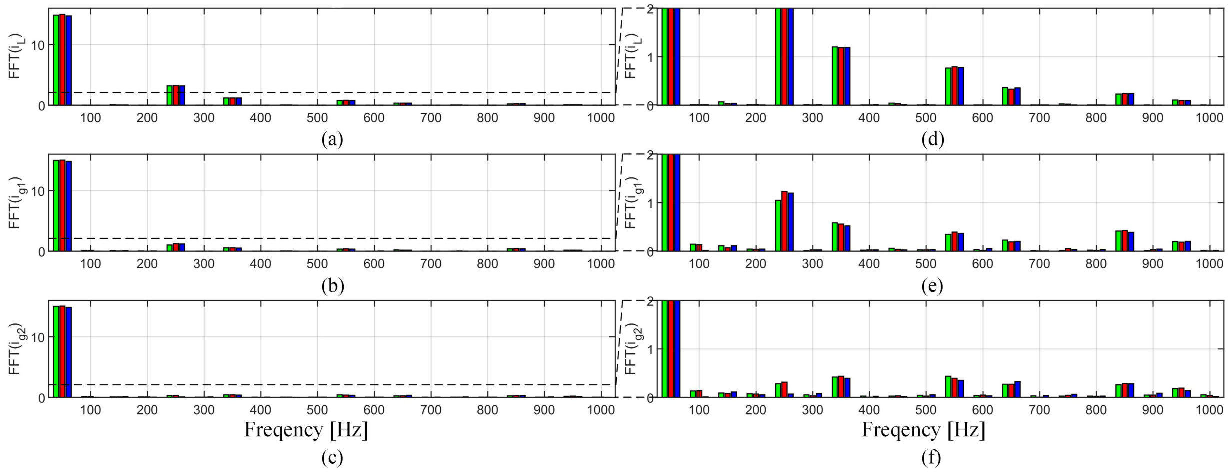

Fig. 18. FFT of the measured currents, (a), (d) i_L – load current, (b), (e) i_{g1} – grid current with only P controller, (c), (f) i_{g2} – grid current with a full PI controller.

a digital-to-analogue converter built in the controller board. Laboratory setup is presented in Fig. 13.

Fig. 14 presents the beginning of the APF operation during experimental tests. Like in simulation results from Fig. 11, DC-bus voltage creation can be noticed at the first and further start of harmonic filtration. It should be noted that the experimental $d'q'$ current contains more distortion than the simulated one. This is caused by several factors neglected in the simulation, like discrete realization of the control and sampling delay (100 μs), measuring noise, dead-time (2.5 μs) applied in the laboratory converter, or grid filter inductor resistance (see Table II).

Steady-state operation of APF is presented in Fig. 15. Moreover, comparison of a classical synchronous reference frame current i_{dq} and a new synchronous reference derived from the vibrating reference frame current i'_{dq} is presented. Despite the distortion, the i'_{dq} current contains a significant share of the DC component in contrast to classical i_{dq}. A negligible share of the fundamental harmonic makes the character of i_{dq} strongly AC. In such a condition the integral controller cannot be accurate due to the finite gain for AC signals. Zero steady-state error requires additional resonant terms. Infinite gain for DC signals ensures accuracy of regulation with the use of the vibrating frame transformation, because all demanded harmonics transform into the DC signal.

The results of current filtration during experimental tests are presented in Figs. 16–18. Although the transformation enables a certain time after load appears, the system filtrates harmonics immediately, which can be seen in Fig. 16, nevertheless further transformation turn on improves APF performance. Fig. 17 presents tests in which APF initially operated only with a proportional controller in the stationary frame and the integration in the vibrating frame was turned on manually.

Integrator outputs I_{out} keeps the DC shape despite the current i'_{dq} distortion. In order to compare operation with a P controller and a full PI controller, fast Fourier transform (FFT) of the load current (the same for both cases) and grid current (separately for each case) is provided in Fig. 18. As can be seen, the transformation gives considerably better results in the filtration of 5$^{\text{th}}$ and 7$^{\text{th}}$ harmonics, but does not influence 11$^{\text{th}}$ and 13$^{\text{th}}$ in comparison to proportional control. Nevertheless, it causes significantly better results in the current THD, as presented in Table IV.

IV. Conclusion

The paper presents an innovative approach to an active power filter control system, using the vibrating reference frame transformation. Thanks to that, APF current which consists mainly of high harmonics may be represented as DC signals in a new $d'q'$ reference frame. Therefore PI controllers may be successfully applied in order to achieve zero steady state APF current error for selected harmonics. Some additional issues were discussed such as load current decomposition necessary for APF reference current assignment and converter current limitation method, which provides apparent power limitation.

Operation of the presented control system was verified in both simulation and experimental tests, which brought satisfactory results. The proposed control system is suitable for implementation in a digital signal processor such as TMS320F28335 used in the experiment and very popular in industry.

Appendix

In general, reference APF current components for the selected harmonics and their derivatives, can be described as:

$$\begin{aligned} i^*_{F\alpha} = {} & |i^*_{F1}|\ \cos(\omega t) + |i^*_{F5}| \cos(5\omega t - \theta_5) \\ & + |i^*_{F7}| \cos(7\omega t - \theta_7) + |i^*_{F11}| \cos(11\omega t - \theta_{11}) \\ & + |i^*_{F13}| \cos(13\omega t - \theta_{13}) \end{aligned} \tag{13a}$$

$$\begin{aligned} i^*_{F\beta} = {} & |i^*_{F1}|\ \sin(\omega t) - |i^*_{F5}| \sin(5\omega t - \theta_5) \\ & + |i^*_{F7}| \sin(7\omega t - \theta_7) - |i^*_{F11}| \sin(11\omega t - \theta_{11}) \\ & + |i^*_{F13}| \sin(13\omega t - \theta_{13}) \end{aligned} \tag{13b}$$

$$\begin{aligned} di^*_{F\alpha} = {} & \omega(- |i^*_{F1}| \sin(\omega t) - 5\,|i^*_{F5}| \sin(5\omega t - \theta_5) \\ & - 7\,|i^*_{F7}| \sin(7\omega t - \theta_7) - 11\,|i^*_{F11}| \sin(11\omega t - \theta_{11}) \\ & - 13\,|i^*_{F13}| \sin(13\omega t - \theta_{13}) \end{aligned} \tag{14a}$$

$$
\begin{aligned}
di^*_{F\beta} = \ & \omega(|i^*_{F1}| \cos(\omega t) - 5\,|i^*_{F5}| \cos(5\omega t - \theta_5) \\
& + 7\,|i^*_{F7}| \cos(7\omega t - \theta_7) - 11\,|i^*_{F11}| \cos(11\omega t - \theta_{11}) \\
& + 13\,|i^*_{F13}| \cos(13\omega t - \theta_{13})
\end{aligned} \tag{14b}
$$

References

[1] P. Bagheri, W. Xu, and T. Ding, "A distributed filtering scheme to mitigate harmonics in residential distribution systems," *IEEE Trans. Power Del.*, vol. 31, no. 2, pp. 648–656, Apr. 2016.

[2] H. Akagi, "Active harmonic filters," *Proc. IEEE*, vol. 93, no. 12, pp. 2128–2141, Dec. 2005.

[3] B. Singh, K. AlHaddad, and A. Chandra, "A review of active filters for power quality improvement," *IEEE Trans. Ind. Electron.*, vol. 46, no. 5, pp. 960–971, Oct. 1999.

[4] H. Akagi, "Modern active filters and traditional passive filters," *Bull. Polish Acad. Sci.*, vol. 54, no. 3, pp. 255–269, 2006.

[5] H. Hu, W. Shi, Y. Lu, and Y. Xing, "Design considerations for DSP-controlled 400 Hz shunt active power filter in an aircraft power system," *IEEE Trans. Ind. Electron.*, vol. 59, no. 9, pp. 3624–3634, Sep. 2012.

[6] C. Lascu, L. Asiminoaei, I. Boldea, and F. Blaabjerg, "High performance current controller for selective harmonic compensation in active power filters," *IEEE Trans. Power Electron.*, vol. 22, no. 5, pp. 1826–1835, Sep. 2007.

[7] C. Lascu, L. Asiminoaei, I. Boldea, and F. Blaabjerg, "Frequency response analysis of current controllers for selective harmonic compensation in active power filters," *IEEE Trans. Ind. Electron.*, vol. 56, no. 2, pp. 337–347, Feb. 2009.

[8] X. Yuan, W. Merk, H. Stemmler, and J. Allmeling, "Stationary-frame generalized integrators for current control of active power filters with zero steady-state error for current harmonics of concern under unbalanced and distorted operating conditions," *IEEE Trans. Ind. Appl.*, vol. 38, no. 2, pp. 523–532, Mar./Apr. 2002.

[9] M. S. Karbasforooshan and M. Monfared, "An improved reference current generation and digital deadbeat controller for single-phase shunt active power filters," *IEEE Trans. Power Del.*, vol. 35, no. 6, pp. 2663–2671, Dec. 2020.

[10] L. Asiminoael, F. Blaabjerg, and S. Hansen, "Detection is key - Harmonic detection methods for active power filter applications," *IEEE Ind. Appl. Mag.*, vol. 13, no. 4, pp. 22–33, Jul./Aug. 2007.

[11] S. Rahmani, N. Mendalek, and K. Al-Haddad, "Experimental design of a nonlinear control technique for three-phase shunt active power filter," *IEEE Trans. Ind. Electron.*, vol. 57, no. 10, pp. 3364–3375, Oct. 2010.

[12] Y. Han, M. M. Khan, L. Xu, G. Yao, L. Zhou, and C. Chen, "A new scheme for power factor correction and active filtering for six-pulse converters loads," *Bull. Polish Acad. Sci.*, vol. 57, no. 2, pp. 157–169, 2009.

[13] O. Vodyakho and C. C. Mi, "Three-Level inverter-based shunt active power filter in three-phase three-wire and four-wire systems," *IEEE Trans. Power Electron.*, vol. 24, no. 5, pp. 1350–1363, May 2009.

[14] J. Chen, X. Zhang, and C. Wen, "Harmonics attenuation and power factor correction of a more electric aircraft power grid using active power filter," *IEEE Trans. Ind. Electron.*, vol. 63, no. 12, pp. 7310–7319, Dec. 2016.

[15] A. K. Dubey, J. P. Mishra, and A. Kumar, "Modified CCF based shunt active power filter operation with dead-band elimination for effective harmonic and unbalance compensation in 3-phase 3-wire system," *IEEE Trans. Power Del.*, vol. 37, no. 3, pp. 2131–2142, Jun. 2022, doi: 10.1109/TPWRD.2021.3104828.

[16] R. Guzman, L. G. de Vicuña, J. Morales, M. Castilla, and J. Miret, "Model-Based control for a three-phase shunt active power filter," *IEEE Trans. Ind. Electron.*, vol. 63, no. 7, pp. 3998–4007, Jul. 2016.

[17] W. Śleszyński, A. Cichowski, and P. Mysiak, "Current harmonic controller in multiple reference frames for series active power filter integrated with 18-pulse diode rectifier," *Bull. Polish Acad. Sci.*, vol. 66, no. 5, pp. 699–704, 2018.

[18] P. Mattavelli, "A closed-loop selective harmonic compensation for active filters," *IEEE Trans. Ind. Appl.*, vol. 37, no. 1, pp. 81–89, Jan./Feb. 2001.

[19] X. Sun, R. Han, H. Shen, B. Wang, Z. Lu, and Z. Chen, "A double-resistive active power filter system to attenuate harmonic voltages of a radial power distribution feeder," *IEEE Trans. Power Electron.*, vol. 31, no. 9, pp. 6203–6216, Sep. 2016.

[20] T. L. Lee and S. H. Hu, "An active filter with resonant current control to suppress harmonic resonance in a distribution power system," *IEEE J. Emerg. Sel. Topics Power Electron.*, vol. 4, no. 1, pp. 198–209, Mar. 2016.

[21] A. Gałecki, M. Michalczuk, A. Kaszewski, B. Ufnalski, and L. M. Grzesiak, "Grid-tied converter operated under unbalanced and distorted grid voltage conditions," *Bull. Polish Acad. Sci.*, vol. 68, no. 2, pp. 389–398, 2020.

[22] S. Wodyk and G. Iwanski, "Vibrating coordinates frame transformation based unity power factor control of a three-phase converter at grid voltage imbalance and harmonics," *IEEE Trans. Ind. Electron.*, vol. 69, no. 2, pp. 1114–1123, Feb. 2022.

Sebastian Wodyk received the M.Sc. degree in electrical engineering from the Faculty of Electrical Engineering, Warsaw University of Technology, Warsaw, Poland, in 2018, where he has been working toward the Ph.D. degree in automation and robotics, since 2018. His research interests include control systems of grid-connected power converters and electrical energy storage systems for renewable energy sources and electrical vehicles.

Grzegorz Iwanski (Senior Member, IEEE) received the M.Sc. degree in automatic control and robotics and the Ph.D. degree in electrical engineering from the Faculty of Electrical Engineering, Warsaw University of Technology (WUT), Warsaw, Poland, in 2003 and 2005, respectively. From 2006 to 2008, he was a Researcher involved with an international project within the Sixth Framework Programme of the European Union, WUT. Since 2009, he has been an Assistant Professor with the Institute of Control and Industrial Electronics, WUT, where he became an Associate Professor in 2019. From 2012 to 2013, he joined the Renewable Electrical Energy System Team, Universitat Politècnica de Catalunya, Barcelona, Terrassa, Spain, within the framework of the scholarship of Polish Minister of Science and Higher Education, Warsaw, Poland. He has coauthored one monograph, three book chapters, and about 80 journal articles and conference papers. His research interests include variable and adjustable speed power generation systems, photovoltaics and energy storage systems, and automotive power electronics and drives. Dr. Iwanski provided two plenary lectures on IEEE technically sponsored international conferences: Ecological Vehicles and Renewable Energies and Joint International Conference on Optimization of Electrical and Electronic Equipment and Aegean Conference on Electrical Machines and Power.